Scanning tunneling co-ramp spectroscopy for reactive adsorbates

Eunyeoung Choi and In-Whan Lyo[*]

Department of Physics, Yonsei University, Seoul, Republic of Korea
(Received 15 August 2011; published 28 November 2011)

We report the development of a spectroscopy for investigating reactive adsorbates, and its application to the study of chemisorbed methoxy on NiAl(110). Conventional scanning tunneling spectroscopy, a powerful tool to study stable adsorbates, is not applicable to the kinds that decompose or desorb upon the exposure to low-energy tunneling electrons. In order to find the electronic structure of these adsorbates, we developed a scanning spectroscopy that minimizes the exposure to external influences. The coramp spectroscopy (CRS), so named by us, involves synchronized ramping-up of bias V and the spatial position in a constant current mode, and recording the tip-sample separation $s(V)$ at the same time. Numerical simulations of $s(V)$ show that the information on the resonance can be extracted from the derivative of $s(V)$. This technique was applied to the investigation of chemisorbed methoxy deposited by the injection of liquid methanol into NiAl(110) surface. It is shown that slow high-bias scans decompose methoxy through C-O bond scission or C-H bond dehydrogenation. Despite such reactivity of methoxy, CRS was successfully applied to reveal that methoxy has a resonance at 3.4 V. Simulations show that the resonance is well separated from the field emission resonances, and attributed to a nonbonding 2e orbital of chemisorbed methoxy. Our technique should be useful in the study of a wide range of molecular adsorbates, particularly, in the study of their unoccupied states where few techniques are available.

I. INTRODUCTION

Molecular adsorption and dissociation on metal and insulator surfaces plays a pivotal role in thin-film growth, passivation and catalysis, even in solar-cell devices. Detailed understanding of chemical states of the adsorbates is thus crucial for such molecule-based applications.[1–4] Considerable progress in understanding of these adsorbates has been made by using scanning tunneling microscopy (STM),[5–8] photoemission spectroscopy,[9] and other methods.[10] However, adsorbed molecules, in many cases intermediate species, are easily perturbed by external influences such as temperature, electric field, and injected charge, as well as photomechanical effect.[11–13] This susceptibility often leads to decomposition, desorption, or intermolecular reactions, which renders it difficult to study intrinsic properties of adsorbates.

Methanol (CH_3OH), industrially synthesized from syngas using Cu-based catalysts, is an attractive source of energy for the hydrogen economy, as the feedstock for direct and reformed methanol fuel cells.[14] In the metal-catalyzed synthesis of methanol as well as its reverse reaction to CO and H, methoxy (CH_3O) is an important intermediate. Dissociative chemisorption of methanol on metal surfaces, in particular, produces methoxy through the scission of the O-H bond, making it an ideal model system for the studies of alcohol chemisorption.

Over the past 30 years, extensive experimental and theoretical studies of methanol and methoxy adsorbed on metallic surfaces have been carried out to characterize their structural and catalytic properties as well as to test new methodologies against the well established adsorbate system. Among the surfaces studied are those of bimetallic alloys such as NiAl[15–19] and Ni_3Al.[18,19] Metallic alloys such as NiAl offer a potential for tuning the electronic and catalytic properties by allowing diverse selections of the surface structures and stoichiometries. In particular, NiAl(110) has a nearly ideal, bulk-terminated structure, almost free of reconstruction, and maintains the bulk

stoichiometry as well, with the Ni and Al atoms arranged in alternating rows.[20,21] Methanol associatively chemisorbs on NiAl(110) at 120 K,[15] and warming to 200 K decomposes methanol through the O-H bond breaking into surface methoxy (CH_3O-),[17,22] which preferentially bonds to only Al sites on the surface, in particular, Al-Al bridge sites.[19] Notably, NiAl(110) breaks the C-O bond of methoxy in an unusually low temperature range of about 300–400 K, compared to monometallic Al or transition metals.[15] At higher temperatures, C-H and C-O bond breakage occurs with the evolution of gaseous H_2, CO, and hydrocarbons including CH_4 in addition to the surface oxygen and carbonaceous species.

While extensive studies on chemisorbed methoxy have been performed experimentally, in particular, as regards to the bonding geometry of methoxy on the surface,[23] there exist few spectroscopic studies of the unoccupied state of chemisorbed methoxy, especially in relation to its role in the decomposition of methoxy.

In this work, we report the investigation of the electronic structure and the decomposition mechanism of methoxy on NiAl(110) surfaces at room temperature by using a unique type of STM-based tunneling spectroscopy. Scanning tunneling spectroscopy (STS) is a powerful tool to map the electronic and vibronic properties of adsorbates in the nanoscale.[7,12] However, as we shall demonstrate, conventional STS is not so useful in studying the intrinsic properties of metastable adsorbates when the low-energy tunneling electrons can induce decomposition or desorption.

Among various kinds of STS, the bias-dependent tip-sample separation $s(V)$ has been frequently employed to study the local surface electrostatic potential by measuring the spatial variation in the field emission resonance (FER), i.e., the image-potential state confined between the sample surface and the trapezoidal tunneling barrier. Since the discovery of FER features in $s(V)$ spectra by Binnig *et al.*[24] and Becker *et al.*,[25] the study of FER had been carried out for a wide

range of systems such as clean surfaces,[26–30] overlayers,[31–34] buried interfaces,[35] molecular adsorbates,[36,37] clusters,[38] and molecular films.[39] On the other hand, $s(V)$ has been less utilized for the study of the electronic structure of surfaces in comparison to I-V spectroscopy, as $s(V)$ responds to the change in the tunneling current logarithmically, hence with a reduced sensitivity.

In order to overcome the limitation of the STS toward metastable adsorbates, we developed a spectroscopic technique that we shall call *co-ramp spectroscopy* (CRS). The CRS allows the characterization of reactive species at the surface in their intrinsic states, by sampling every part of a spectrum $s(V)$ on different, fresh molecules before they decompose or desorb. By employing the CRS, we were able to measure and identify an unoccupied state resonance responsible for the direct decomposition of methoxy species. This tool should be applicable to most of highly reactive molecules, whose states may be otherwise inaccessible by any other spectroscopies.

II. EXPERIMENTAL METHODS

The experiments were performed in an ultrahigh vacuum chamber equipped with a home-made STM of the Besocke beetle type,[40,41] with a base pressure of 5×10^{-11} mbar. Home-built control electronics and software were used to operate the STM. A NiAl(110) sample was cleaned by repeated cycles of Ne ion sputtering (1.5 kV for 60 min) and subsequent annealing (1300 K for 5 min).[42] Methanol was directly injected to the sample surface by using a pulse valve (Parker Pulse Valve series 9) mounted on the UHV chamber.[43,44] Opening and closing cycles of the pulse valve filled with methanol (purity 99.98 %, HPLC grade) were driven by a computer-controlled power supply for a precision control, and the subsequent burst and decay of the chamber pressure following the injection was continuously monitored for the numerical integration and conversion to an equivalent gaseous methanol dose. The placement of the substrate surface from the pulse valve was varied from 50 to 150 mm. The methanol inside the pulse valve was pumped not only to purge ambient gases, but also to maintain the background pressure to the low equilibrium pressure of about 100 mbar. All experiments were performed at room temperature by using chemically etched W tips.

III. RESULTS AND DISCUSSION

STM images of a clean NiAl(110) surface revealed atomically flat and clean terraces with no defects, as presented in Fig. 1(a). An injection of the 2-L equivalent of liquid methanol onto the NiAl(110) produced a highly homogeneous surface macroscopically, although at atomic scale the surface was covered with the poorly coordinated molecular species, as shown in Fig. 1(b) and the inset. The species are attributed to methoxy molecules formed by the scission of the O-H bond of methanol. The molecular species were found very reactive to the injection of high-bias electrons. Figures 1(c) and 1(d) show the contrasting behavior of adsorbates following the high-bias scan of opposite polarity. A high-positive-bias (>5 V) scan over the methoxy-covered surface gave rise to a large modification of the adsorbates as shown in Figs. 1(d)
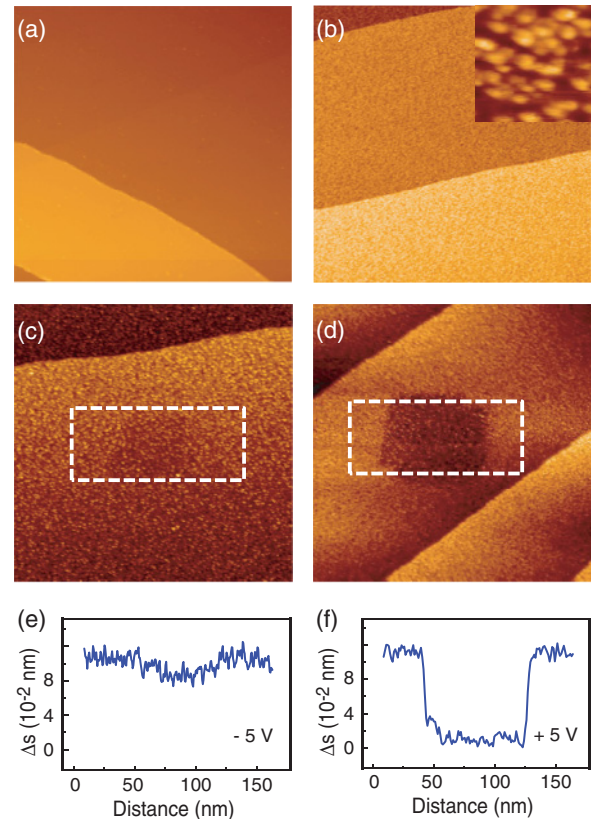

FIG. 1. (Color online) STM images of (a) clean NiAl(110) and (b) methoxy-covered surface after the 7-L methanol injection (size 270×270 nm^2), with the inset showing the atomic detail (size 7×7 nm^2). Imaging conditions are $V_S = 0.5$ V and $I_t = 0.1$ nA. (c)–(d) Images taken after high bias (+5 V) stress scans of negative and positive polarities within the dashed boxes respectively. (e)–(f) Horizontally averaged line profiles of the boxed areas of (c) and (d). (Imaging condition: $V_S = 0.5$ V, $I_t = 0.1$ nA, and image size 270×270 nm^2.)

and 1(e). On the other hand, a negative-bias scan produced little change to the scanned area as shown in Figs. 1(c) and 1(e). Thus it is clear that the positive bias modifies the surface whereas the negative bias does not. The amount of modification was also strongly dependent on the current as well as the bias.

In order to investigate the details of the reaction, a smaller amount of methanol was injected by shortening the duration of the valve opening to produce isolated adsorbates. Figure 2(a) shows a typical image of methoxy adsorbates thus produced on the surface, with topographic corrugation of about 0.20–0.25 nm that is higher than any other extrinsic defects such as water, carbon contaminants, which have typically 0.05 to 0.1 nm corrugations. In order to see if isolated molecules exhibit similar behavior as in Fig. 1, bias stress tests were performed on each molecule. When two methoxy molecules were subjected to a long and high voltage stress (+4 V and 100 pA for 1 s), two different types of decomposition products were observed. One type decreased in the height by about 0.05 nm [R in Fig. 2(b)], and the other type suffered more drastically by 0.15 nm [L in Fig. 2(c)]. Two dissimilar responses to the same stress are ascribed to different decomposition pathways. Methoxy
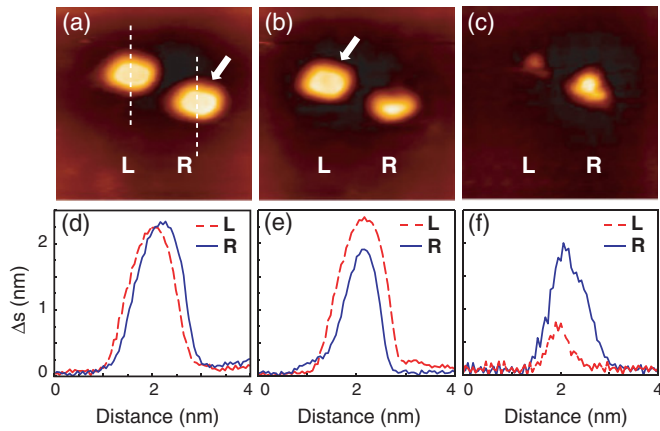
FIG. 2. (Color online) Topographic STM images of two methoxy adsorbates on NiAl(110) before and after high-bias stresses (scan condition: $V_S = 2.0$ V, $I_t = 0.1$ nA, and image sizes 6.7×6.7 nm^2). Labels L and R denote the left and the right adsorbates, respectively. (a) A pair of pristine methoxy adsorbates. (b) The same pair after a positive high-bias pulse (+4 V and 1 s width) was applied to the adsorbate pointed by white arrow in (a). (c) The same pair after another identical pulse was applied to the adsorbate pointed by white arrow in (b). (d), (e), and (f) Cross-sectional line profiles of the corresponding adsorbates along the dotted lines in (a), (b), and (c), respectively. Dashed red and solid blue lines represent adsorbates L and R, respectively.

has two low-reaction barrier pathways of decomposition, C-O bond scission and dehydrogenation of C-H bonds.[45] Between these two, the C-O bond scission would entail drastic change to the STM image by producing two low-corrugation products of CH$_3$ and O on the surface, compared with the dehydrogenation pathway. Therefore the large change associated with L in Fig. 2(c) is best assigned to the C-O bond scission process.[18,19] This result clearly shows that the adsorbed methoxy species are reactive and readily decompose to other minor species by the electron injection. There are also secondary reactions to cause further decompositions of C-H bonds under a continuous injection of electrons. With the tip height fixed, however, the rate of these decompositions would decrease precipitously, as the tunneling current falls exponentially after the first decomposition by the high-bias pulse. Thus the cascade of decomposition events does not ensue.

Scanning tunneling spectroscopy is a tool well suited to reveal the chemical states of the molecular species through probing the local density of states (LDOS) of the molecule with subangstrom spatial resolution. However, any unstable molecular species can easily foil the effort to collect the spectrum. The structural or configurational modification of a molecular species during the spectroscopic measurement would result in distorted, spurious data. For instance, Fig. 3 shows the results of STS over three different methoxy molecules on a NiAl(110) surface. Clearly, the STS spectra are not reproducible, and they indicate that the interaction with the adsorbates could commence at a bias as low as 1.6 eV.

In order to overcome such difficulties, we devised the CRS scheme that allows the measurement of the molecular states in the unmodified state; each CRS scan consists of simultaneously ramping the voltage for lateral tip positioning
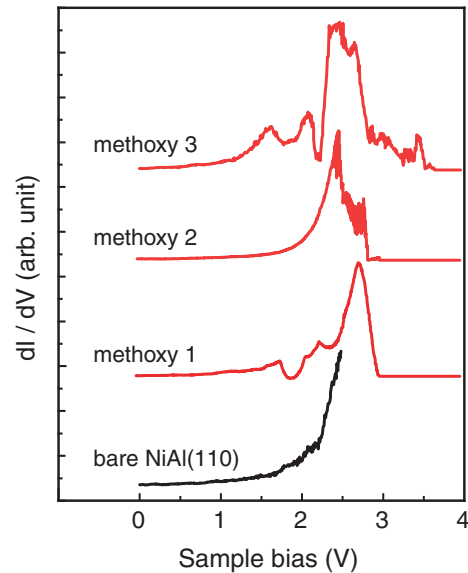

FIG. 3. (Color online) Typical *I-V* spectra of three different methoxy molecules on a NiAl(110) surface (reference condition: $V_S = 0.5$ V and $I_t = 0.1$ nA). Positive bias ramps dissociate the molecules and give rise to irreproducible spectra.

and the sample bias in synchronization, with the feedback loop operating in the constant-current mode. At each regularly spaced location and incremented (or decremented) bias during the co-ramping, a tip height variation is recorded as a data point of the CRS spectrum, as schematically depicted in Fig. 4(a). Thus the tip visits a *fresh* new location with different sample bias for each and every data point of a CRS spectrum. In this way, when the tip height is read for a CRS data acquisition, the molecule under the tip is guaranteed not to have undergone any modification previously by the spectral bias. In practice, in order to reduce the fluctuation in the data, one needs to obtain the ensemble average of CRS spectra, which is done by taking CRS spectra along many different fresh paths and averaging them after subtracting the topographic background. The downside to the CRS is the loss of spatial resolution, as each spectrum is necessarily an average of spectra from different parts of the molecule as well as the exposed substrate. We will show that the tradeoff is worthwhile, since the CRS provides information on the molecular species for the first time, otherwise unavailable.

The CRS thus minimizes the probability of decomposition. In comparison, the ordinary STS subjects a single molecule to the entirety of the bias sweep from low to high bias, providing the ample opportunity for methoxy to decompose. One should also note that the CRS is, in principle, a time-resolved technique. In the decomposition bias range, the extent of how much time the STM tip dwells over a site is expected to affect the probability of decomposition of a single methoxy molecule by either charge or energy transfer. In a typical STM imaging procedure, the tip spends a preset duration of time over a single spot of interest to allow the feedback circuit to adjust the tip-sample gap distance before reading the gap distance and moving to the next spot to start anew. The *dwell time*, as we will call, is the critical factor to influence the degree of decomposition during the acquisition of a CRS
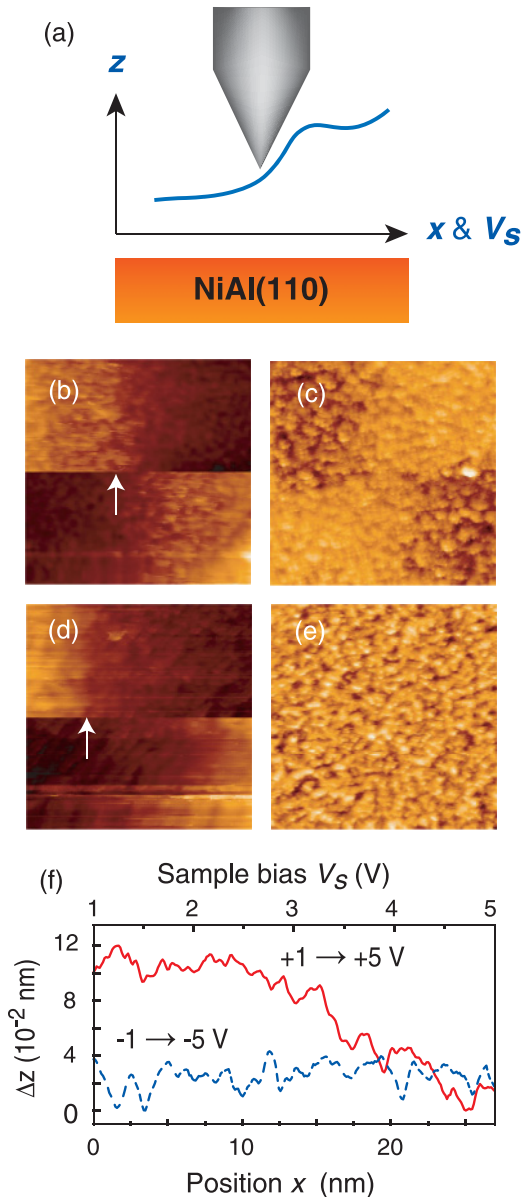
FIG. 4. (Color online) (a) A schematic diagram of the CRS. The bias V_S and the lateral tip position x are linearly coramped to form a bias ramp $V_S(x)$ under the constant tunneling current condition. The trajectory (blue line) of the tip is recorded as $s(V_S(x))$. (b) An image representation of CRS data obtained by incremental ($+1 \rightarrow +5$ V) and decremental ($+5 \rightarrow +1$ V) bias ramps in the lower and the upper halves respectively. (c) A post-CRS image of the same area as (b). (d) An image representation of CRS data obtained by decremental ($-1 \rightarrow -5$ V) and incremental ($-5 \rightarrow -1$ V) bias ramps in the lower and the upper halves, respectively. (e) A post-CRS image of the same area as (c). A dwell time of 1 ms was used in (b) and (d). Arrows mark the bright-to-dark contrast thresholds. Imaging conditions are 0.5 V and 0.1 nA with the image size of 27×27 nm^2. (f) Averaged line profiles of the lower half of the images (c) and (e) in solid red and dotted blue lines, respectively.

spectrum. Thus, in principle, one should be able to probe the rate of decomposition of methoxy molecules by systematically varying the dwell time. Namely, as a methoxy molecule is subjected to a decomposition bias for an increasingly longer

period, then there is the correspondingly higher probability that it decomposes within the time window and lowers the tip height. By mapping the dwell time versus the gap distance, one may obtain energy-dependent lifetimes of reactive states of molecules.

Figures 4(b) and 4(d) show CRS spectra taken on methoxy-adsorbed NiAl(110) surfaces in the image representation. The CRS spectra were taken with a sufficiently long dwell time (1 ms) deliberately to cause the decomposition of molecules so that the bias-dependent modifications can be topographically imaged. The spectra were taken both in forward and backward directions in bias to check the scan direction dependence. In the image representations, any difference between two CRS data appears superficial due to the rising background, with the exception of the shift in the positions of dark-to-bright thresholds as indicated by arrows in Figs. 4(b) and 4(d). Forward and backward CRS scan images appear symmetric to each other, indicating it is independent of the CRS scan direction. On the other hand, the topographic images obtained subsequent to the CRS show remarkable differences. The topographic image taken after the positive-bias CRS scan went dark [see Fig. 4(c)] or on a downward slope [see Fig. 4(f)] from the location corresponding to about 2.6 V in the positive-bias CRS scan. In contrast, the topographic image taken after the negative-bias CRS scan indicates no sign of any changes [see Fig. 4(e)]. These data show that the decomposition of methoxy begins from a bias higher than 2.6 V, whereas no similar chemical reaction occurs at a negative bias of the same range.

Figure 5 makes a comparison between the CRS spectra of a methoxy-covered and a clean NiAl(110) surfaces, after removing the background obtained by a 0.5-V constant-current-mode topographic image. The spectra were taken
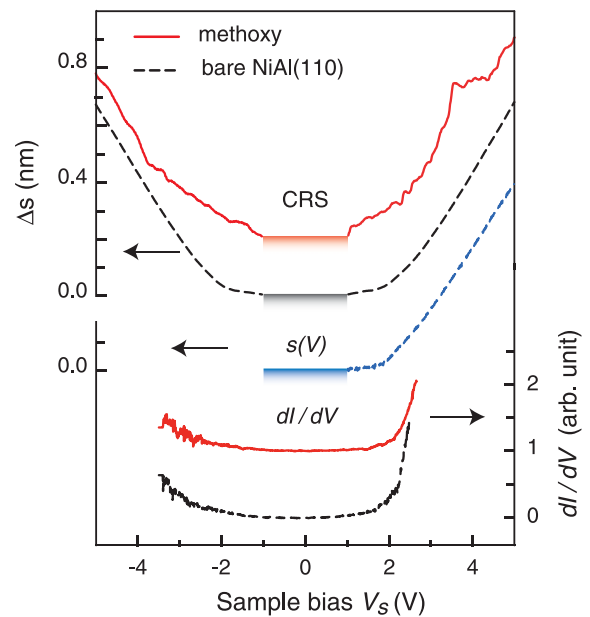

FIG. 5. (Color online) Comparisons of CRS, conventional $s(V)$, and $\partial I/\partial V$ spectra on methoxy-adsorbed (solid red line) and pristine (dashed line) NiAl(110). CRS and $\partial I/\partial V$ spectra are shifted vertically for clear view. The bias range where CRS data were not taken to avoid the tip crash is shaded in gradient. Reference tunneling condition: $V_S = 0.5$ V and $I_t = 0.1$ nA.

with a minimal dwell time to avoid the decomposition over methoxy adsorbates. Let us consider the case of the clean NiAl surface first. Its CRS spectra show that the tip-sample distance goes through a smooth monotonous increase all the way to high bias. The CRS spectra appear highly symmetric to bias polarity. In Fig. 5, also shown is a spectrum of conventional tip-sample separation $s(V)$, that is, taken on a single site. Not surprisingly, the conventional $s(V)$ and the CRS spectra of the pristine surface look almost identical, which assures us that the two spectroscopies are equivalent over the same, homogeneous surface. In the case of the methoxy-covered surface, for negative bias up to -4 eV, only a featureless, linear increase in the tip-sample distance is observed. Small features appearing between -4.0 and -5.0 V are attributed to a FER. On the other hand, the positive-bias CRS spectrum on the methoxy-adsorbed surface, as shown in Fig. 5, exhibits a distinct peak at $+3.6$ V that rides on the smooth background similar to that in the negative-bias side.

An analysis of the CRS spectra in Fig. 5 indicates that the $+3.6$ eV CRS feature is unrelated to the FER. If the feature should be related to a FER, it would correspond to only the lowest order ($m=1$) FER, for usual values of tip and sample work functions. On clean metal surfaces, the $m=1$ FER typically turns up in $s(V)$ either weak or weakly steplike,[24,25,28–30] and the chemisorption of atoms or molecules merely shifts the energetic position of the $m=1$ FER, driven by the change in the tunnel barrier.[24,36] Thus, if the CRS feature should originate from the FER, then a counterpart ought to be present in the CRS spectrum of the clean NiAl(110) surface as well. However, as Fig. 5 clearly shows, no such feature is found within the bias window, implying that the $m=1$ FER is either too weak or well out of range to be observed in CRS spectra of the clean NiAl(110) surface. As shown in Fig. 5, the conventional $s(V)$ spectrum of the clean NiAl(110) exhibit a dismissively weak feature below 5 V, and the first steplike one at 6.3 V, although the latter is not shown here. This means that whichever feature corresponds to the $m=1$ FER, it is irrelevant to the 3.6 V CRS feature either by the intensity or the position. The lack of shared features between the two CRS spectra, besides the featureless backgrounds, thus entails that the FER is not the origin of the CRS feature.

In order to understand the experimental results, we performed model calculations to simulate the CRS spectra as well as conventional I-V spectra to check for the consistency. We simulated CRS spectra by numerically solving the one-dimensional Schrödinger equation and mapping the tip-sample distance $s(I_0, V)$ that produces an identical tunneling current I_0 as a function of bias.

In the model, the tip-sample distance s is the distance between the two electrodes, with the tip at $z=0$, the sample at $z=s$, and the image plane at $z=s_i<s$. The electric potential $U(z,s)$ between the two parallel electrodes is then calculated by taking into account the image potential, the applied bias voltage V_s, and the work functions of the tip and the sample, ϕ_t and ϕ_s, by using the expression[34,46,47]

$$U(z,s) = \frac{-e^2}{4\pi\epsilon_0 s_i} g(x) - (eV_s + \Delta\phi)\frac{z}{s}, \qquad (1)$$

which uses the dimensionless variable $x \equiv z/s_i$ and the contact potential $\Delta\phi \equiv \phi_t - \phi_s$. The function $g(x)$ expresses

x-dependent image potential for multiple images between the two electrodes.

At high bias, the asperity region of the tip contributing to tunneling broadens in the constant current mode as the electric field becomes less localized, and thus the tip would be located farther away from the surface than the predictions made by strictly one-dimensional model calculations. In our simulation, this effect was assumed linear and incorporated by scaling the simulated $s(V)$ to the experimental CRS spectrum for the best fitting result. The resulting tip-sample distance variation in total was about 0.5 nm before the scaling, compared to the experimental value of about 0.7 nm between 1 and 5 V as shown in Fig. 6(a). The work functions used were 3.57 eV for the sample and 5.2 eV for the W tip. A simulated CRS spectrum is shown in Fig. 6(a) in comparison with the experimental data. The inset shows an excellent fit between the simulated and the experimental CRS spectra after subtracting the same background, simulated by using a uniform LDOS.

Perplexing as it may seem at first, the peak appearing in the simulated CRS spectrum of Fig. 6(a) and the inset is *not* a real one that represents a resonance proper, and consequently neither is the peak in the experimental CRS data. We explain the origin of the pseudopeak in the following analysis. In a simple model using an average barrier,[48–51] the tunneling current $I(s,V)$ is related to the tip-sample distance s and the tip-sample bias potential V through the equation

$$I(s,V) \propto \int_0^V d\epsilon\, \rho_t(E_F + \epsilon - V)\rho_s(E_F + \epsilon)e^{-2\kappa(\epsilon,V)s},$$
$$(2)$$

where ρ_t and ρ_s are the LDOS associated with the tip and the sample, and the extinction coefficient $\kappa(E,V) \propto [2(\phi - E) + V]^{1/2}$ is a measure of the wave-function decay away from the surface, with ϕ the average work function. For the discussion purpose and without loss of generality, we consider the sample LDOS consisting of a single Lorentzian peak LDOS $\rho_{s,p}(E)$ and a uniform background LDOS $\rho_{s,b}$, as shown in Fig. 6(b), with each component generating tunneling current I_p and I_b, respectively. An assumption of a uniform ρ_t for the tip state, a sufficiently narrow $\rho_{s,p}(E)$, and a slowly varying κ allows approximating the Lorentzian part of the tunneling current I_p by

$$I_p(s,V) \propto e^{-2\kappa_p s} \int_0^V d\epsilon\, \rho_{s,p}(E_F + \epsilon), \qquad (3)$$

where E_p is the energy of the Lorentzian peak and $\kappa_p \equiv \kappa(E_p, V)$ is the extinction coefficient at E_p. It is easy to see that the integral in Eq. (3) yields an inverse tangent function of V, and similarly for the uniform background part of the tunneling current I_b an exponential function. Thus, as Fig. 6(b) shows, the simulated I-V spectrum is essentially the sum (black solid line) of a steplike inverse tangent function and an exponential function (red dashed line). The relationship between the two components I_p and I_b can be also verified in the semilogarithmic plot of the I-V spectrum in Fig. 6(b). Note that the semilogarithmic plot of the I-V spectrum exhibits strong qualitative resemblance to the CRS spectra in Fig. 6(a), reflecting the relation $I(s) \sim \exp(-2\kappa s)$ or $\ln I(s,V) \propto s(V)$. The top curve in Fig. 6(b) shows the recovered LDOS through
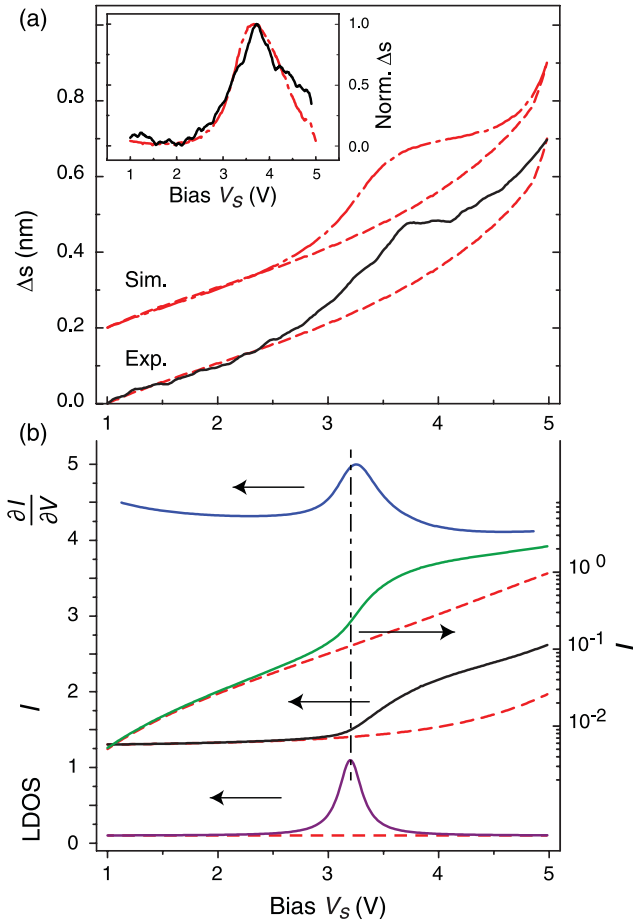
FIG. 6. (Color online) CRS spectra vs a conventional *I-V* spectrum. (a) Comparison between the simulated and the experimental CRS spectra presented by the dot-dashed (red) and the solid (black) curves, respectively. The inset shows the same simulated and experimental CRS spectra after subtracting the dashed (red) background. (b) Recovery of LDOS by *I-V* spectroscopy. An *I-V* spectrum (second-to-bottom black line) was calculated from the combined LDOS (bottom purple line) of a Lorentzian peak and a uniform background LDOS, which is shown in the linear (second-to-bottom black line) and the logarithmic (second-from-top green line) scales, together with its derivative $\partial I/\partial V$ (top blue line). Each arrow points to the axis and the physical description of the corresponding curve. The vertical dot-dashed line marks the position of the peak in the sample LDOS. In both plots, dashed red lines represent spectra owing to the uniform background LDOS only. Unless specified, units are arbitrary.
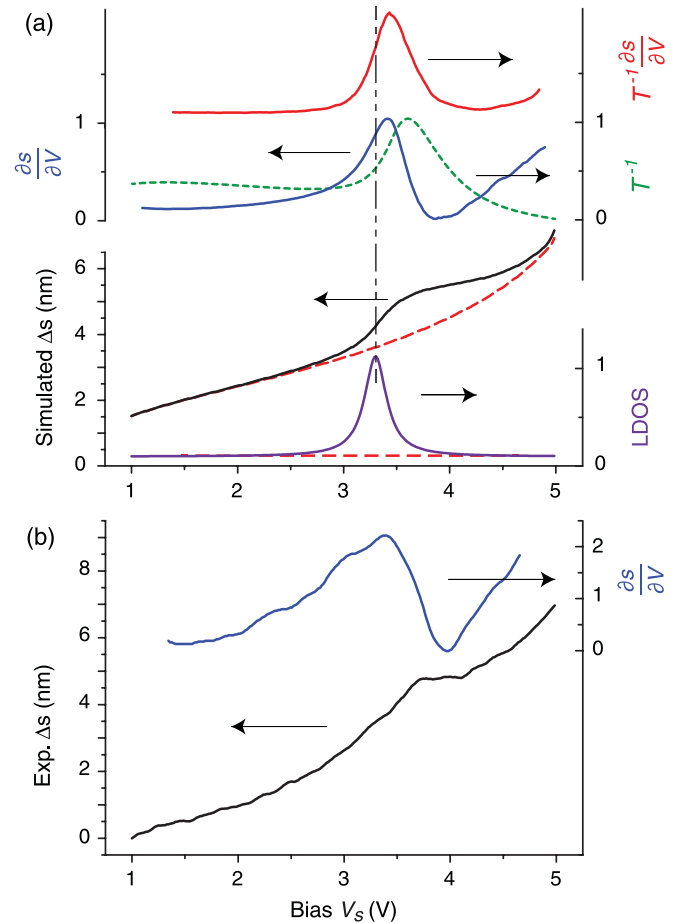
FIG. 7. (Color online) Comparisons of (a) simulated and (b) experimental bias-dependent tip-sample distances $s(V)$ and their $\partial s/\partial V$ data. Each arrow points to the axis and the physical description of the corresponding curve. In (a), dashed (red) curves represent the cases of a uniform LDOS (bottom). The second-to-bottom (black) curve denotes $s(V)$, which was calculated from the combined LDOS of a Lorentzian peak of 3.3 V and the uniform background as shown at the bottom. The second-from-top solid (blue) curve represents $\partial s/\partial V$ data of the simulated CRS spectra. Second-from-top dotted (green) and top solid (red) curves stand for the inverse transmission factor T^{-1}, and the product of T^{-1} and $\partial s/\partial V$, respectively. The vertical line marks the position of the peak in the sample LDOS. In (b), bottom (black) and top (blue) curves denote the CRS spectrum $s(V)$ and its derivative $\partial s/\partial V$, respectively. Units are arbitrary, unless specified.

the typical method of differentiating the *I-V* spectrum. The fidelity of the reproduced LDOS to the original indicates the level of consistency in our numerical calculations.

The origin of the pseudopeak is thus clear. The pseudopeak stems from the opening of a new tunneling channel such as a resonance state whose contribution to the tunneling current rises initially as more states in the resonance become available, and then declines at higher bias as tunneling is relegated to the deeper-lying electrons facing the increasing higher tunneling barrier. Therefore *peaking* of the pseudopeak, if ever, does not occur at the resonance state, but at the crossover point between these two trends.

Figure 7(a) shows a CRS spectrum, obtained by tracing the tip-sample distances $s(V)$ that maintain an identical tunneling current for a series of bias voltages. Again, the input sample LDOS for the simulation comprises two parts, a Lorentzian peak and a uniform background, which is shown as the bottom curve in Fig. 7(a). The recovery of the LDOS from the CRS spectra cannot be done in the same manner as conventional *I-V* spectra, as the CRS spectra are taken at the constant *I*. We devised a new method to extract the LDOS out of the CRS spectra, which is to take the first derivative of the CRS spectrum with bias. The result is shown as the dot-dashed (red) curve in Fig. 6(a), which closely resembles the original input LDOS at the bottom of the plot.

The reason why the scheme works at all is as follows. Differentiating Eq. (2) with respect to V and imposing the condition $\partial I/\partial V = 0$ yields

$$\rho_s(E_F + V) \; \propto \; e^{2\kappa s} \; \left.\frac{\partial s}{\partial V}\right|_{I(s,V)}, \qquad (4)$$

where $\kappa(V)$ is assumed to vary slowly. Equation (4) shows that two factors, the inverse transmission factor $T^{-1} \equiv \exp(2\kappa s)$ and the derivative of the tip-sample distance $\partial s/\partial V$, are the two main components of the sample LDOS ρ_s. They are driven by $s(V)$, which is strongly dependent on bias as demonstrated in Fig. 6(a). In order to weigh ρ_s's dependence on the two factors, each factor was calculated separately by using the simulated CRS spectrum and the results are plotted in Fig. 7(a). The curves show that the inverse transmission factor exhibits a symmetric resonance behavior, whereas $\partial s/\partial V$ displays a typical antisymmetric behavior for being the derivative of essentially the same, symmetric resonance, which is another form of the pseudoresonance discussed earlier. As Eq. (4) dictates, the product of two factors [top red curve in Fig. 7(a)] successfully recovers the LDOS, although there exists a slight blue shift in the peak position in the product spectrum, similar to Fig. 6(a). The blue shift is the reflection of the pseudo peak in Δs through the inverse transmission factor. And this is the level of accuracy typical in this kind of analysis.[48] On the other hand, the LDOS can be recovered via Eq. (4) only if the *a priori* knowledge of the inverse transmission factor T^{-1} is available. Lacking the information, one may still choose another approach of ignoring the inverse transmission factor T^{-1} altogether in Eq. (4) and instead rely only on $\partial s/\partial V$, the antisymmetric curve. This is not unreasonable, because the peak positions of $\partial s/\partial V$ and the product curves should coincide when the width of the Lorentzian LDOS vanishes.

With this in mind, the same procedure was applied to the experimental CRS data to extract the LDOS, with the result shown in Fig. 7(b). Similar to the peak positions 3.4 and 3.3 V given by $\partial s/\partial V$ of the simulated spectrum and the full spectrum fitting, respectively, the experimental $\partial s/\partial V$ data display a broad curve with the peak located at 3.4 V. The experimental $\partial s/\partial V$ curve also exhibits an antisymmetric behavior, in accordance with the analysis. The low-energy tail in the curve could be associated with the C-H bond breaking pathways of methoxy. For instance, on Cu surfaces, the pathway has a decomposition barrier about 1/3 lower than that for the C-O bond breaking.[52–54] In this case, although the bond breaking may appear at low bias, the experimental CRS signature would be low, as Δs is small for the C-H bond breakage, as noted earlier.

The adsorption of methanol on NiAl(110) lowers the work function by ~ 1.6 eV,[15] because of strong polarity in the molecule. This raises the possibility that the CRS peak may correspond to the $m = 1$ state of an FER. We calculated the FER spectra by using the same method, noting the theoretical work function of 5.17 eV for clean NiAl(110).[55] The peak positions of the FER were sensitive to the types of the image charge models, but less so with the initial tip-sample distance. Under an identical condition but the Lorentzian LDOS, it was found that the lowest energy peak in the FER, obtained from the peaks in $\partial s/\partial V$, was located at 4.4 eV or higher above the Fermi level, depending on the details of the model. In fact, the upwardly curved tail ends of the CRS spectra near 5 V in bias in Figs. 6(a) and 7(a) represent the lead part of the $m = 1$ FER that trails the CRS resonance. Therefore it is concluded that the FER is not its origin.

We now discuss the CRS peak in terms of a molecular origin. The existence of the 3.4-eV peak is consistent with the observations made in Figs. 2, 3, and 4 that the high-bias stress decomposes the adsorbates. The presence of the well localized 3.4-eV peak strongly suggests that the decomposition is a resonance phenomenon. Two different orbitals of methoxy are relevant to the resonance. One is a partially unoccupied $2e$ orbital, i.e., the highest occupied molecular orbital (HOMO), and the other is a $6a_1$ orbital, i.e., the lowest unoccupied molecular orbitals (LUMO). The $2e$ orbital is a largely oxygen p-type lone pair mixed with an antibonding C-O π^* orbital. On the other hand, the $6a_1$ orbital has mainly the character of a C-O σ^* state. Previous photoemission studies[15,18,56] of CH_3O on metal surfaces assigned the state with the binding energy of 5–6 eV to the occupied $2e$ state. On the other hand, a near-edge x-ray absorption fine structure (NEXAFS) study of methoxy on Ni and Cu surfaces assigned peak *A* to the transition of $O1s \rightarrow 2e$ and peak *B* that is located ~ 5 eV above peak *A* to the transition of $O1s \rightarrow 6a_1$.[57] In the case of CO chemisorption on metal surfaces, peak *A* corresponds to the excitation of an electron from $O1s$ to the antibonding 2π state, which lies above the vacuum level in the unperturbed chemisorbed state.[58] Upon the creation of a core hole in $O1s$ by x-ray adsorption, the 2π state is pulled down by ~ 5 eV close to the Fermi level because of the increased Coulomb interaction with the core. Conversely, peak *A* in NEXAFS would indicate the existence of a low-lying unoccupied π orbital near the Fermi level. Despite the lack of NEXAFS data in the literature, similar final-state effects are expected for methoxy on NiAl surfaces as well. Under the supposition, the 3.4-eV resonance in CRS spectra would then correspond to the unoccupied part of the $2e$ orbital above the Fermi level. This state may be brought about by the hybridization of methoxy $2e$ orbital with Al $3sp$ states in the combined ionic and covalent bonding to NiAl surfaces, similar to other metals.[18,56] The alternative assignment of the CRS resonance would be the LUMO. However, the LUMO of methoxy lies much higher, 5 eV higher than the unoccupied $2e$ orbital in the cases of Cu and Ni, well beyond the CRS resonance.[57,59]

The dissociation energy of chemisorbed methoxy is substantially lower than the CRS resonance energy. The calculated activation energy for the scission of the C-O bond by tilting is about ~ 1.6 eV on Al[60] and Cu surfaces.[53,54] In comparison, the photodissociation energy threshold for the reaction $CH_3O \rightarrow CH_3 + O$ in gas phase is 3.81 eV.[61] Thus the C-O bond of chemisorbed methoxy is significantly weakened compared to that of gas phase, partly owing to the occupation of the $2e$ orbital by charge transfer from the substrate.[59] The additional occupation of the $2e$ orbital by a tunneling electron would further weaken the C-O bond, facilitating the scission of the C-O bond in accordance with our experimental observations.

IV. CONCLUSIONS

In summary, we developed a spectroscopy that allows the investigation of reactive molecules. CRS reduces the decomposition or desorption of adsorbates by taking new data from fresh molecules. The resultant CRS spectrum is a bias-dependent tip-sample separation $s(V)$ at constant current. Through numerical simulations, we showed that $\partial s(V)/\partial V$ recovers the essence of the sample LDOS. We studied chemisorbed methoxy on NiAl(110) surface, which was produced by the pulsed injection of liquid methanol. High-bias stress to individual molecules produces two different decomposition pathways attributed to scission of C-O bonds and dehydrogenation. The application of CRS to methoxy adsorbates exhibited a resonance state at 3.4 eV in the unoccupied state. Simulations show that the resonance is not an FER, and it is attributed to a nonbonding $2e$ orbital of chemisorbed methoxy. Expanding on the already powerful capability of scanning tunneling spectroscopy, the CRS provides new opportunities to explore a wide range of reactive molecules for catalysis and device applications.

*lyo@yonsei.ac.kr

[1] W. Ho, J. Chem. Phys. **117**, 11033 (2002).

[2] X. D. Cui, A. Primak, X. Zarate, J. Tomfohr, O. F. Sankey, A. L. Moore, T. A. Moore, D. Gust, G. Harris, and S. M. Lindsay, Science **294**, 571 (2001).

[3] C.-H. Chung, W.-J. Jung, and I.-W. Lyo, Phys. Rev. Lett. **97**, 116102 (2006).

[4] V. Iancu and S.-W. Hla, Proc. Natl. Acad. Sci. USA **103**, 13718 (2006).

[5] S.-W. Hla and K.-H. Rieder, Annu. Rev. Phys. Chem. **54**, 307 (2003).

[6] Q. H. Wang and M. C. Hersam, Nano Lett. **11**, 589 (2011).

[7] K. Motobayashi, Y. Kim, H. Ueba, and M. Kawai, Phys. Rev. Lett. **105**, 076101 (2010).

[8] L. Scudiero, D. E. Barlow, U. Mazur, and K. W. Hipps, J. Am. Chem. Soc. **123**, 4073 (2001).

[9] D. Weier, T. Lühr, A. Beimborn, F. Schönbohm, S. Döring, U. Berges, and C. Westphal, Surf. Sci. **604**, 1608 (2010).

[10] M. J. Ford, R. C. Hoft, and J. D. Gale, Mol. Simul. **32**, 1219 (2006).

[11] J. R. Hahn and W. Ho, J. Chem. Phys. **131**, 044706 (2009).

[12] X. H. Qiu, G. V. Nazin, and W. Ho, Phys. Rev. Lett. **93**, 196806 (2004).

[13] M. J. Comstock, N. Levy, A. Kirakosian, J. Cho, F. Lauterwasser, J. H. Harvey, D. A. Strubbe, J. M. J. Fréchet, D. Trauner, S. G. Louie, and M. F. Crommie, Phys. Rev. Lett. **99**, 038301 (2007).

[14] D. R. Palo, R. A. Dagle, and J. D. Holladay, Chem. Rev. **107**, 3992 (2007).

[15] B.-R. Sheu, S. Chaturvedi, and D. R. Strongin, J. Phys. Chem. **98**, 10258 (1994).

[16] B. R. Sheu and D. R. Strongin, J. Catal. **154**, 379 (1995).

[17] S. Chaturvedi and D. R. Strongin, J. Phys. Chem. B **102**, 2970 (1998).

[18] Ø. Borck, I.-H. Svenum, and A. Borg, Surf. Sci. **603**, 2378 (2009).

[19] I.-H. Svenum, Ø. Borck, K. Schulte, L. Walle, and A. Borg, Surf. Sci. **603**, 2370 (2009).

[20] M. H. Kang and E. J. Mele, Phys. Rev. B **36**, 7371 (1987).

[21] X. Torrelles, F. Wendler, O. Bikondoa, H. Isern, W. Moritz, and G. R. Castro, Surf. Sci. **487**, 97 (2001).

[22] M. Bowker and F. Leibsle, Catal. Lett. **38**, 123 (1996).

[23] M. K. Bradley, D. Kreikemeyer Lorenzo, W. Unterberger, D. A. Duncan, T. J. Lerotholi, J. Robinson, and D. P. Woodruff, Phys. Rev. Lett. **105**, 086101 (2010).

[24] G. Binnig, K. H. Frank, H. Fuchs, N. Garcia, B. Reihl, H. Rohrer, F. Salvan, and A. R. Williams, Phys. Rev. Lett. **55**, 991 (1985).

[25] R. S. Becker, J. A. Golovchenko, and B. S. Swartzentruber, Phys. Rev. Lett. **55**, 987 (1985).

[26] T. Jung, Y. W. Mo, and F. J. Himpsel, Phys. Rev. Lett. **74**, 1641 (1995).

[27] K. Bobrov, A. J. Mayne, and G. Dujardin, Nature (London) **413**, 616 (2001).

[28] P. Wahl, M. A. Schneider, L. Diekhöner, R. Vogelgesang, and K. Kern, Phys. Rev. Lett. **91**, 106802 (2003).

[29] J. I. Pascual, C. Corriol, G. Ceballos, I. Aldazabal, H.-P. Rust, K. Horn, J. M. Pitarke, P. M. Echenique, and A. Arnau, Phys. Rev. B **75**, 165326 (2007).

[30] D. B. Dougherty, P. Maksymovych, J. Lee, M. Feng, H. Petek, and J. T. Yates, Phys. Rev. B **76**, 125428 (2007).

[31] J. A. Kubby, Y. R. Wang, and W. J. Greene, Phys. Rev. Lett. **65**, 2165 (1990).

[32] A. J. Caamaño, Y. Pogorelov, O. Custance, J. Méndez, A. Baró, J. Veuillen, J. Gómez-Rodríguez, and J. Sáenz, Surf. Sci. **426**, L420 (1999).

[33] H.-C. Ploigt, C. Brun, M. Pivetta, F. Patthey, and W.-D. Schneider, Phys. Rev. B **76**, 195404 (2007).

[34] P. Ruffieux, K. Aït-Mansour, A. Bendounan, R. Fasel, L. Patthey, P. Gröning, and O. Gröning, Phys. Rev. Lett. **102**, 086807 (2009).

[35] J. A. Kubby and W. J. Greene, Phys. Rev. Lett. **68**, 329 (1992).

[36] D. B. Dougherty, P. Maksymovych, J. Lee, and J. T. Yates, Phys. Rev. Lett. **97**, 236806 (2006).

[37] A. Pronschinske and D. B. Dougherty, J. Phys. Chem. Lett. **1**, 2613 (2010).

[38] S. Stepanow, A. Mugarza, G. Ceballos, P. Gambardella, I. Aldazabal, A. G. Borisov, and A. Arnau, Phys. Rev. B **83**, 115101 (2011).

[39] D. Dougherty, P. Maksymovych, J. Lee, and J. Yates Jr., Chem. Phys. Lett. **431**, 303 (2006).

[40] K. Besocke, Surf. Sci. **181**, 145 (1987).

[41] B. C. Stipe, M. A. Rezaei, and W. Ho, Rev. Sci. Instrum. **70**, 137 (1999).

[42] W. Song and M. Yoshitake, Appl. Surf. Sci. **241**, 164 (2005).

[43] H. Tanaka, C. Hamai, T. Kanno, and T. Kawai, Surf. Sci. **432**, L611 (1999).

[44] L. Grill, I. Stass, K.-H. Rieder, and F. Moresco, Surf. Sci. **600**, L143 (2006).

[45]R. Neubauer, C. M. Whelan, R. Denecke, and H.-P. Steinrük, Surf. Sci. **507-510**, 832 (2002).

[46]G. Binnig, N. Garcia, H. Rohrer, J. M. Soler, and F. Flores, Phys. Rev. B **30**, 4816 (1984).

[47]J. Bono and R. H. Good Jr., Surf. Sci. **188**, 153 (1987).

[48]N. D. Lang, Phys. Rev. B **34**, 5947 (1986).

[49]I.-W. Lyo and P. Avouris, Science **245**, 1369 (1989).

[50]M. Grobis, A. Wachowiak, R. Yamachika, and M. F. Crommie, Appl. Phys. Lett. **86**, 204102 (2005).

[51]G. Buchs, P. Ruffieux, P. Gröning, and O. Gröning, Appl. Phys. Lett. **93**, 073115 (2008).

[52]S. Sakong and A. Groß, J. Catal. **231**, 420 (2005).

[53]L. Xu, D. Mei, and G. Henkelman, J. Chem. Phys. **131**, 244520 (2009).

[54]D. Mei, L. Xu, and G. Henkelman, J. Phys. Chem. C **113**, 4522 (2009).

[55]J. I. Lee, C. L. Fu, and A. J. Freeman, Phys. Rev. B **36**, 9318 (1987).

[56]M. Witko, K. Hermann, D. Ricken, W. Stenzel, H. Conrad, and A. M. Bradshaw, Chem. Phys. **177**, 363 (1993).

[57]K. Amemiya, Y. Kitajima, Y. Yonamoto, S. Terada, H. Tsukabayashi, T. Yokoyama, and T. Ohta, Phys. Rev. B **59**, 2307 (1999).

[58]J. Stöhr and R. Jaeger, Phys. Rev. B **26**, 4111 (1982).

[59]D. Zeroka and R. Hoffmann, Langmuir **2**, 553 (1986).

[60]L. T. Sein Jr. and S. A. Jansen, J. Phys. Chem. B **102**, 2415 (1998).

[61]D. L. Osborn, D. J. Leahy, and D. M. J. Neumark, J. Chem. Phys. A **101**, 6583 (1997).